UDC 544.526.5:546.26-162:628.3

Gozzal Sidrasulieva [a], Nuritdin Kattaev [a], Khamdam Akbarov [a], Altinay Aytmuratova [a], Sarbinaz Usnatdinova [a], Jaykhun Mamatov [a], Sardorbek Otajonov [a], Rayhona Muyassarova [b], Sadatdin Tileubaev [c]

FACILE SYNTHESIS AND PHYSICOCHEMICAL PROPERTIES OF OXYGEN-DOPED GRAPHITIC CARBON NITRIDE (O-g-C_3N_4) FOR EFFICIENT PHOTOCATALYTIC DEGRADATION OF METHYLENE BLUE

[a] Department of Chemistry, National University of Uzbekistan, Tashkent, Uzbekistan
[b] Department of Inorganic, Physical and Colloidal Chemistry, Tashkent Pharmaceutical Institute, Tashkent, Uzbekistan
[c] Department of Organic and Inorganic Chemistry, Karakalpak State University, Nukus, Uzbekistan

A metal-free oxygen-doped graphitic carbon nitride (O-g-C_3N_4) photocatalyst was synthesized via a facile one-step thermal polycondensation of melamine followed by ultrasonic dispersion. The obtained O-g-C_3N_4 exhibited a pseudo-layered structure and nanoscale morphology. The optical band gap was determined to be 2.64 eV, indicating visible-light activity. The photocatalytic performance was evaluated through the degradation of methylene blue under solar irradiation, achieving nearly complete degradation within 120 min. Kinetic analysis revealed that the process follows a pseudo-first-order model with a rate constant of 0.018 min^{-1}. The enhanced photocatalytic activity is attributed to oxygen-induced modification of the electronic structure and improved charge separation. The results demonstrate that O-g-C_3N_4 is an efficient metal-free photocatalyst for wastewater treatment applications.

Keywords: O-g-C_3N_4, nanoparticles, morphology, photocatalysis, methylene blue, visible light, wastewater treatment.

DOI: 10.32434/0321-4095-2026-167-4-30-42

Introduction

In recent decades, the contamination of water resources by anthropogenic organic compounds has become a critical environmental issue. A wide range of hazardous substances, including dyes, pharmaceuticals, surfactants, pesticides, and other industrial chemicals, have been detected in both wastewater and natural water systems. Many of these pollutants are characterized by high toxicity, persistence, and resistance to biodegradation, posing serious risks to ecosystems and human health [1–6].

Synthetic organic compounds represent a major class of water pollutants due to their continuous release from industrial, agricultural, and domestic sources. Even at low concentrations, these compounds can exhibit mutagenic, carcinogenic, and endocrine-disrupting effects. Therefore, the development of efficient, environmentally friendly, and cost-effective technologies for water purification is of great importance [7–10].

Conventional treatment methods, such as adsorption, coagulation, membrane filtration, and

electrochemical processes, have been widely applied for pollutant removal. However, these techniques often suffer from several limitations, including high operational cost, incomplete mineralization, and the generation of secondary pollutants [11–14]. In this regard, advanced oxidation processes (AOPs), particularly heterogeneous photocatalysis, have attracted increasing attention due to their ability to generate reactive oxygen species capable of degrading organic pollutants into harmless end products under light irradiation [15–18].

Titanium dioxide (TiO_2) has been extensively studied as a photocatalyst because of its chemical stability, non-toxicity, and low cost. However, its wide band gap restricts its activity to the ultraviolet region, which significantly limits the utilization of solar energy. Therefore, the development of visible-light-active photocatalysts is highly desirable [19,20].

Graphitic carbon nitride (g-C_3N_4) has emerged as a promising metal-free semiconductor due to its suitable band structure, high thermal and chemical stability, and facile synthesis from nitrogen-rich precursors such as melamine. Owing to its moderate band gap, g-C_3N_4 can absorb visible light and has been widely investigated in photocatalytic applications, including organic pollutant degradation [21–24]. Nevertheless, pristine g-C_3N_4 suffers from rapid recombination of photogenerated electron–hole pairs and relatively low photocatalytic efficiency.

To overcome these limitations, various modification strategies have been developed, among which heteroatom doping is considered an effective approach. In particular, oxygen doping can significantly modify the electronic structure of g-C_3N_4, introduce defect sites, and enhance charge separation efficiency, thereby improving photocatalytic performance under visible light [25–29].

In this work, nanosized oxygen-doped graphitic carbon nitride (O-g-C_3N_4) was synthesized via thermal polycondensation of melamine in air. The physicochemical properties of the material were systematically investigated, and its photocatalytic activity was evaluated through the degradation of methylene blue under solar irradiation. Particular attention was paid to the kinetic behavior of methylene blue degradation and the role of oxygen doping in enhancing photocatalytic performance.

Materials and methods

Materials

Melamine ($C_3H_6N_6$, 99%), isopropyl alcohol (C_3H_7OH, 96%), distilled water, and methylene blue (MB) were used as starting materials. All chemicals were of analytical grade and used without further purification.

Synthesis of O-g-C3N4 photocatalyst

Oxygen-doped graphitic carbon nitride (O-g-C_3N_4) was synthesized via a facile one-step thermal polycondensation of melamine.

Melamine was placed into a sealed autoclave without prior degassing. The synthesis was carried out in the presence of air, without using an inert atmosphere. After loading, the autoclave was tightly closed and subjected to thermal treatment at 500^{0}C for 3 h.

During the thermal process, melamine underwent polycondensation, leading to the formation of a graphitic carbon nitride structure. The presence of air in the closed system is assumed to promote the incorporation of oxygen-containing functional groups into the structure, resulting in oxygen doping.

After cooling, the obtained product was dispersed in a water–isopropanol medium and treated ultrasonically for 6 h using a UM-2 ultrasonic disperser (Unitra Unimasz Olsztyn, Poland) operating at 50 kHz to obtain nanosized particles.

Characterization techniques

The structural, morphological, thermal, and optical properties of the synthesized material were investigated using a set of physicochemical methods.

FTIR spectra were recorded using a Bruker spectrometer (Bruker, Germany) in the range of 400–4000 cm^{-1} using KBr pellets prepared by pressing the sample with potassium bromide.

Phase composition was analyzed by X-ray diffraction (XRD) using an X'Pert PRO diffractometer (Malvern Panalytical, Netherlands) with CuKα radiation (λ=1.54056 Å). The measurements were performed in the 2θ range of 10–80^0 with a scanning step of 0.01^0.

Surface morphology and elemental composition were examined by scanning electron microscopy combined with energy-dispersive X-ray spectroscopy (SEM-EDX) using a JSM-IT200LA microscope (JEOL Ltd., Japan).

Particle size and internal structure were analyzed by transmission electron microscopy (TEM) using a CM30 microscope (Philips, Netherlands).

Optical properties were investigated by UV–Vis diffuse reflectance spectroscopy using an EMC-30PC-UV/VIS spectrometer (Germany).

Photoluminescence (PL) spectra were recorded in the wavelength range of 300–1100 nm using a Cary Eclipse fluorescence spectrophotometer (Agilent Technologies, USA).

Thermal stability was studied by thermogravimetric analysis (TGA/DTG) using a DTG-60 instrument (Shimadzu, Japan) under argon atmosphere in the temperature range of 30–900^{0}C with a heating rate of 10^{0}C/min and a sample mass

of approximately 10 mg.

Photocatalytic activity tests

The photocatalytic activity of O-g-C_3N_4 was evaluated by the degradation of MB in aqueous solution under solar irradiation.

For the experiment, 0.5 g of the photocatalyst was dispersed in 500 mL of MB solution. Prior to irradiation, the suspension was stirred in the dark for 15 min to establish adsorption–desorption equilibrium.

During the photocatalytic reaction, 2 mL aliquots were withdrawn every 15 min, centrifuged to remove solid particles, and analyzed spectrophotometrically.

The concentration of MB was determined using a UV-5100 UV–Vis spectrophotometer (Metash Instruments Co., Ltd., China).

Kinetic analysis

The photocatalytic degradation kinetics of methylene blue was analyzed using zero-order, first-order, and second-order kinetic models. The experimental data were fitted using the following equations:

$$C_0 - C = k_0 t,$$

$$\ln\left(\frac{C_0}{C}\right) = k_1 t,$$

$$\frac{1}{C} = k_2 t + \frac{1}{C_0}.$$

where C_0 and C are the initial and current concentrations of the dye, respectively; k_0, k_1, and k_2 are the rate constants of zero-, first-, and second-order reactions, respectively; and t is the reaction time.

Results and discussion

FTIR analysis

The structural features of the synthesized oxygen-doped graphitic carbon nitride (O-g-C_3N_4) were investigated using Fourier transform infrared (FTIR) spectroscopy. The obtained spectrum exhibits characteristic absorption bands confirming the formation of a polymeric graphitic carbon nitride framework with oxygen-containing functional groups (Fig. 1).

A broad absorption band observed at ~3157 cm^{-1} is attributed to the stretching vibrations of $-NH_2$, $-NH$, and $-OH$ groups. The presence of this band indicates residual amino functionalities as well as hydroxyl groups, which may originate from incomplete polycondensation of melamine and the incorporation of oxygen during synthesis in an air-containing environment.

A distinct band at ~802 cm^{-1} corresponds to the breathing mode of the tri-s-triazine (heptazine) units, which is a typical fingerprint of graphitic carbon nitride. This confirms the formation of a condensed heterocyclic structure.

Strong absorption bands located at ~1315 and ~1229 cm^{-1} are assigned to the stretching vibrations of C–N–C and C–NH–C linkages in the polymeric network. These bands indicate the formation of a conjugated structure characteristic of g-C_3N_4. Additional bands at ~1568 and ~1624 cm^{-1} are attributed to the stretching vibrations of C=N bonds and aromatic heterocycles within the heptazine framework.

The band at ~887 cm^{-1} can be associated with

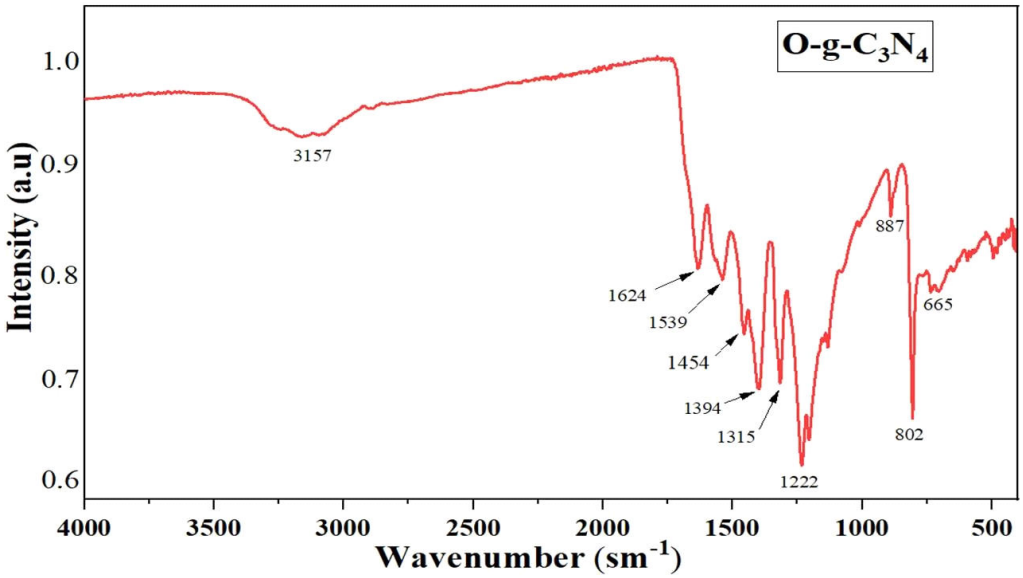

Fig. 1. FTIR spectrum of oxygen-doped graphitic carbon nitride (O-g-C_3N_4)

vibrations of the six-membered heterocyclic ring, while the weak band at ~665 cm^{-1} corresponds to deformation vibrations of amino groups. Low-frequency bands observed at ~473 and ~667 cm^{-1} are related to skeletal vibrations of the condensed heterocyclic structure.

Overall, the FTIR results confirm the successful formation of oxygen-doped graphitic carbon nitride. The presence of characteristic heptazine units, C—N and C=N bonds, along with oxygen- and hydrogen-containing functional groups, is consistent with the proposed structure of O-g-C_3N_4 synthesized via thermal treatment of melamine in a sealed air environment.

XRD analysis

The crystal structure of the synthesized oxygen-doped graphitic carbon nitride (O-g-C_3N_4) was investigated by X-ray diffraction (XRD). The diffraction pattern exhibits two characteristic reflections located at $2\theta \approx 13.27^0$ and 27.17^0, which correspond to the (100) and (002) crystallographic planes, respectively (Fig. 2).

The diffraction peak at ~13.27^0 is attributed to the in-plane structural ordering of tri-s-triazine (heptazine) units, indicating the periodic arrangement of the fundamental building blocks within the polymeric network. The more intense peak at ~27.17^0 corresponds to the interlayer stacking of the conjugated aromatic structure, which is typical for graphitic carbon nitride materials and reflects the layered nature of the material.

The observed diffraction pattern is consistent with previously reported data for g-C_3N_4 and confirms the formation of a pseudo-layered structure. The relatively broad diffraction peaks indicate a low degree of crystallinity and suggest the presence of nanosized crystallites.

The crystallite size of O-g-C_3N_4 was estimated using the Scherrer equation based on the broadening of diffraction peaks. The calculated crystallite sizes for different reflections are presented in Table 1. The results show that the dominant fraction of crystallites is in the range of ~3.9—6.0 nm, with the most intense peak at $2\theta \approx 27.17^0$ corresponding to a crystallite size of approximately 3.92 nm.

In addition, crystallites with sizes of approximately 5—6 nm are also observed, while a minor fraction of larger crystallites (~18.6 nm) appears at higher diffraction angles. This distribution indicates a polydisperse structure with predominantly nanoscale domains. Such structural features are favorable for photocatalytic applications, as reduced crystallite size can enhance surface reactivity and facilitate charge transfer processes.

Overall, the XRD results confirm the successful formation of oxygen-doped graphitic carbon nitride with a layered structure composed of nanosized crystallites.

UV—Vis diffuse reflectance and band gap analysis

The optical properties of the synthesized O-g-C_3N_4 photocatalyst were investigated using UV—Vis diffuse reflectance spectroscopy (DRS), as shown in Fig. 3a. The obtained spectrum demonstrates significant absorption in the visible region, indicating the ability of the material to be activated under solar

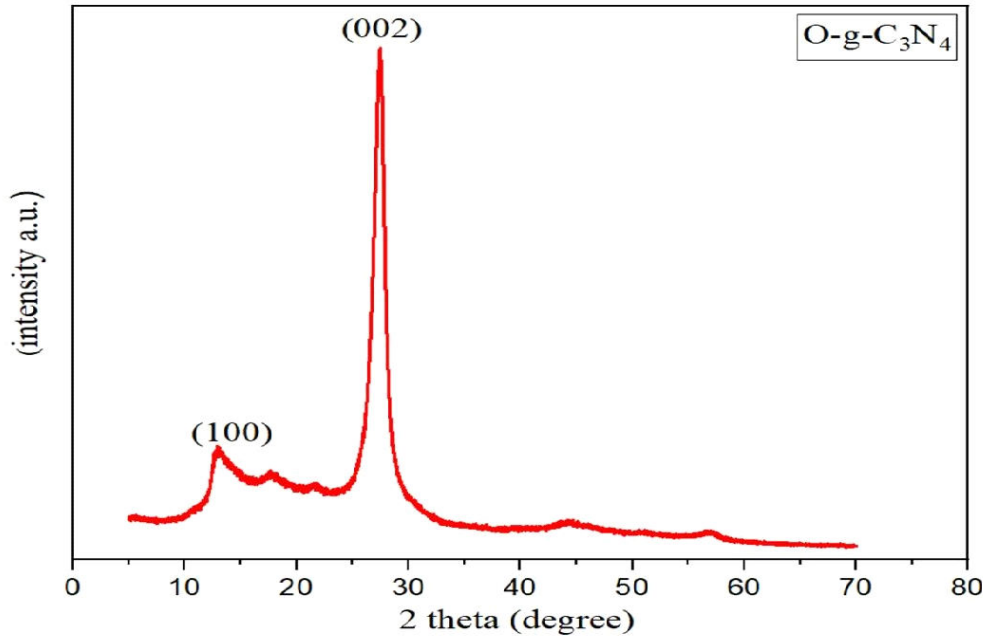

Fig. 2. XRD pattern of oxygen-doped graphitic carbon nitride (O-g-C_3N_4)

irradiation.

The optical band gap energy (E_g) was estimated using the Kubelka–Munk function derived from the diffuse reflectance data and further analyzed by the Tauc plot method, as shown in Fig. 3b. The relationship between photon energy (hν) and the transformed reflectance function was used to determine the band gap energy.

The calculated band gap of O-g-C_3N_4 was found to be approximately 2.64 eV, which is characteristic of graphitic carbon nitride and confirms its semiconductor nature. This value indicates that the synthesized material is active in the visible light region, making it suitable for photocatalytic applications under solar irradiation.

The relatively narrow band gap compared to conventional wide-band-gap photocatalysts allows for enhanced light absorption and improved utilization of the solar spectrum. In addition, oxygen doping is expected to introduce defect states and modify the electronic structure, which can facilitate charge carrier separation and reduce recombination rates.

As a result, the observed optical properties of O-g-C_3N_4 contribute to its enhanced photocatalytic performance in the degradation of organic pollutants.

SEM and TEM analysis

The morphology and microstructure of the synthesized O-g-C_3N_4 were investigated using scanning electron microscopy (SEM) and transmission electron microscopy (TEM).

The SEM images at different magnifications (Fig. 4a–d) reveal that the material exhibits a heterogeneous and irregular morphology composed of agglomerated particles with layered and plate-like features. At lower magnifications (Fig. 4a,b), the sample appears as loosely packed aggregates, while at higher magnifications (Fig. 4c,d), a more developed structure consisting of interwoven sheet-like and partially elongated features is observed.

Such morphology is attributed to the release of gaseous products (e.g., NH_3) during the thermal polycondensation of melamine, followed by structural rearrangement. The presence of wrinkled and stacked layers indicates the formation of a graphitic-like structure with a certain degree of disorder, which is typical for g-C_3N_4 materials.

The EDX spectra (Fig. 4e,f) confirm that the material is mainly composed of carbon and nitrogen, with a small amount of oxygen, indicating successful incorporation of oxygen into the g-C_3N_4 framework. The detected oxygen is associated with doping and the formation of oxygen-containing functional groups during synthesis in an air-containing environment.

TEM analysis (Fig. 5a–c) provides further insight into the internal structure of the material. The images reveal the presence of nanoscale structures with partially elongated and tubular-like morphology. In particular, individual tubular-like features with diameters on the order of ~8 nm can be observed (Fig. 5a,b). However, these structures are not uniformly distributed and appear together with irregular nanoscale domains, indicating a predominantly disordered nanostructured framework.

The formation of such tubular or fiber-like features may be associated with local structural rearrangement during thermal treatment and subsequent ultrasonic dispersion. Overall, the material consists mainly of nanosized domains with a heterogeneous structure.

The presence of nanoscale features and structural disorder implies a high density of defect sites, which can act as active centers and facilitate charge separation. These characteristics are favorable for enhancing the photocatalytic activity of O-g-C_3N_4.

Particle size distribution (DLS analysis)

The particle size distribution of the synthesized O-g-C_3N_4 was analyzed using dynamic light scattering (DLS). The results (Fig. 6a,b) indicate that the material exhibits a bimodal size distribution.

The dominant fraction of particles is centered at approximately 30.6 nm, accounting for about 86% of the total population. A secondary fraction with a larger average size of approximately 176.7 nm contributes about 13–14%, which can be attributed to particle aggregation in the suspension.

The presence of larger particles is likely associated with the formation of agglomerates in the water–alcohol medium, as well as the development of a solvation shell around the particles. As a result, the

Table 1

Crystallite size of O-g-C_3N_4 calculated using the Scherrer equation

No.	2θ (^{0})	d (E)	I/I? (%)	β (FWHM)	D (nm)
1	13.27	6.665	34	1.384	6.04
2	24.97	3.563	18	1.455	5.84
3	27.17	3.279	100	2.181	3.92
4	29.52	3.023	13	1.500	5.72
5	77.43	1.232	10	0.572	18.59

hydrodynamic diameter measured by DLS is typically larger than the actual particle size observed by TEM.

The bimodal distribution indicates that the synthesized material consists predominantly of nanoscale particles with partial aggregation. Such structural characteristics are typical for g-C_3N_4-based materials obtained via thermal condensation and subsequent ultrasonic dispersion.

TGA/DTG analysis

The thermal stability and composition of the synthesized O-g-C_3N_4 were investigated by thermogravimetric analysis (TGA) and differential thermogravimetric analysis (DTG). The corresponding thermograms are presented in Fig. 7.

The TGA curve shows that the material exhibits relatively high thermal stability up to approximately 500–540^{0}C, indicating the formation of a stable polymeric structure characteristic of graphitic carbon nitride.

In the temperature range of 56–531^{0}C, a gradual

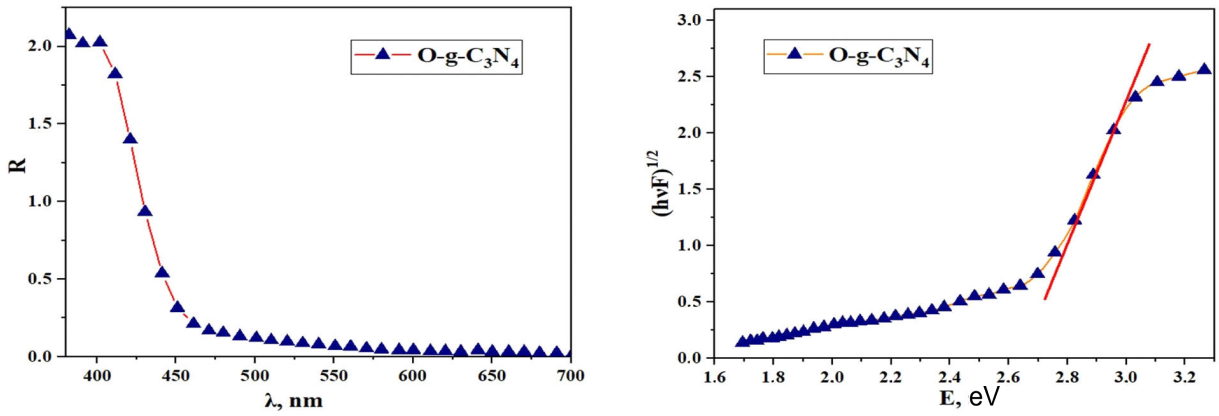

(a) (b)

Fig. 3. (a) UV–Vis diffuse reflectance spectrum of O-g-C_3N_4; (b) Tauc plot for band gap determination

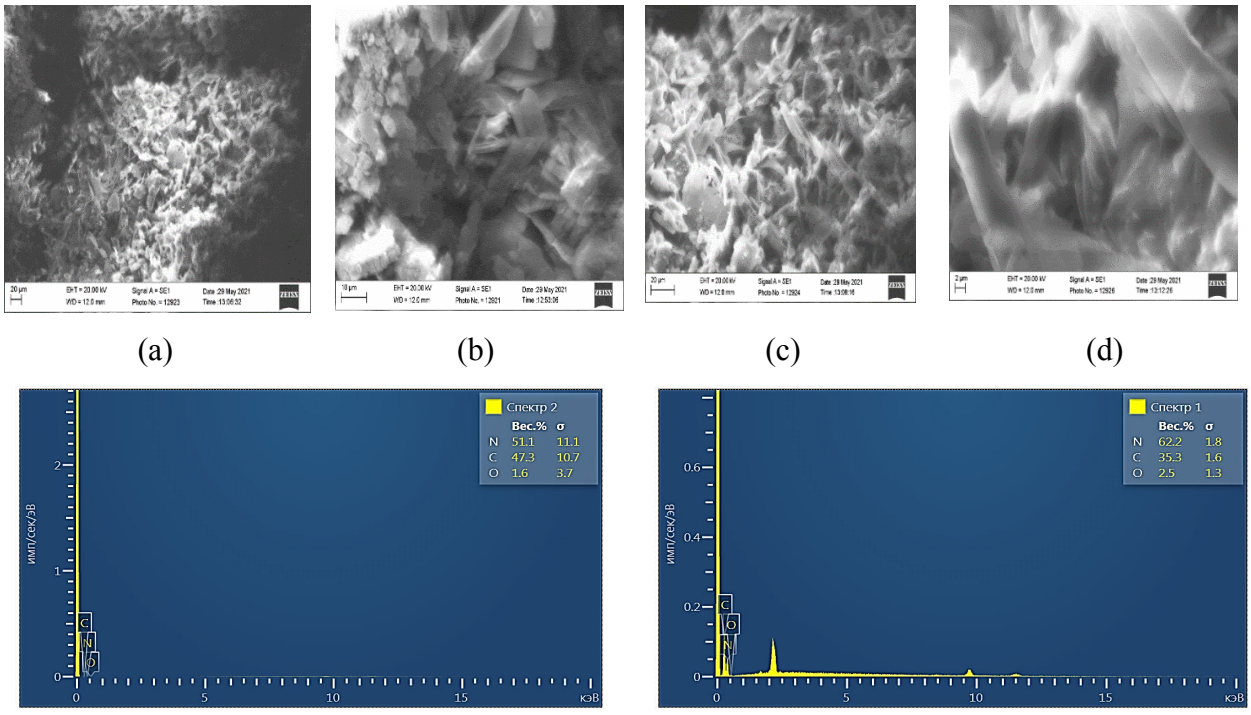

(a) (b) (c) (d)

(e) (f)

Fig. 4. SEM images of O-g-C_3N_4 at different magnifications: (a) ×200; (b) ×500; (c) ×1000; (d) ×2000; (e) and (f) corresponding EDX spectra

weight loss is observed, which can be attributed to the removal of physically adsorbed species, residual intermediates, and incomplete condensation products. This stage is accompanied by endothermic processes, indicating structural rearrangement and further condensation of the polymeric network.

A significant and rapid mass loss occurs in the temperature range of 542–684^{0}C, corresponding to the thermal decomposition of the g-C_3N_4 framework. This stage is associated with the breakdown of the conjugated nitrogen–carbon structure and the release of gaseous products such as NH_3 and other nitrogen-containing species.

The total weight loss during the decomposition process reaches approximately 82.1%, which is consistent with the thermal degradation behavior of polymeric carbon nitride materials.

The DTG curve shows a pronounced peak in the high-temperature region, confirming that the main decomposition occurs within a relatively narrow temperature interval. This behavior indicates a well-formed but thermally decomposable polymeric structure.

Overall, the thermal analysis demonstrates that O-g-C_3N_4 possesses sufficient thermal stability for photocatalytic applications under ambient and moderate temperature conditions. The decomposition temperature is consistent with previously reported values for g-C_3N_4 materials.

Photocatalytic activity

The photocatalytic activity of the synthesized O-g-C_3N_4 was evaluated by the degradation of

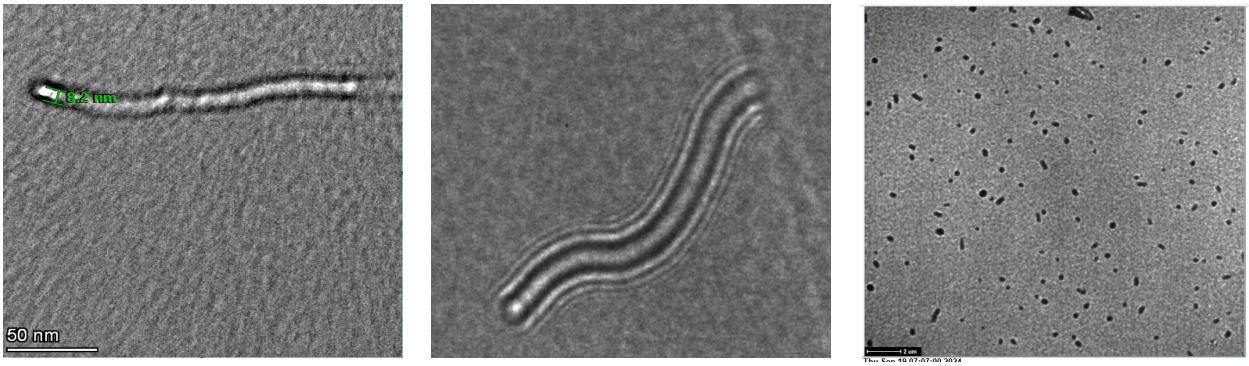

(a) (b) (c)

Fig. 5. TEM images of O-g-C_3N_4: (a) and (b) tubular-like nanostructures (~8 nm diameter); (c) distribution of nanosized domains

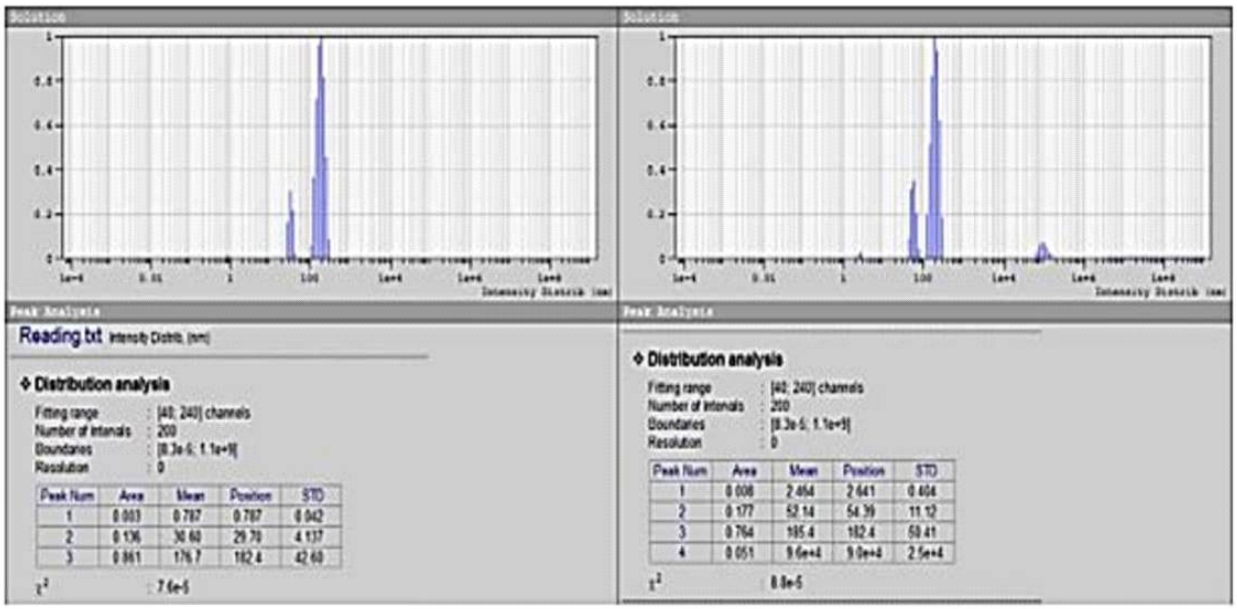

Fig. 6. Particle size distribution of O-g-C_3N_4 obtained by DLS: intensity distribution and size distribution analysis

methylene blue (MB) in aqueous solution under different irradiation conditions, including UV, visible, and solar light. The variation of MB concentration with irradiation time is presented in Fig. 8.

Prior to irradiation, the suspension was stirred in the dark for 15 min to establish adsorption–desorption equilibrium. The results indicate that the decrease in MB concentration during this stage was negligible, confirming that adsorption plays a minor role in the overall removal process.

As shown in Fig. 8, the photocatalytic degradation efficiency strongly depends on the irradiation source. In the absence of the photocatalyst, only a slight decrease in MB concentration was observed, indicating that photolysis alone is insufficient for effective degradation.

In contrast, the presence of O-g-C_3N_4 significantly enhances the degradation rate. Among the tested irradiation conditions, the highest photocatalytic activity is observed under solar irradiation, followed by UV and visible light. Under solar light, the concentration of methylene blue decreases rapidly, reaching nearly complete degradation within 120 min.

This enhanced performance can be attributed to the ability of O-g-C_3N_4 to absorb a broad range of light due to its band gap energy of 2.64 eV, enabling efficient utilization of visible light. Additionally,

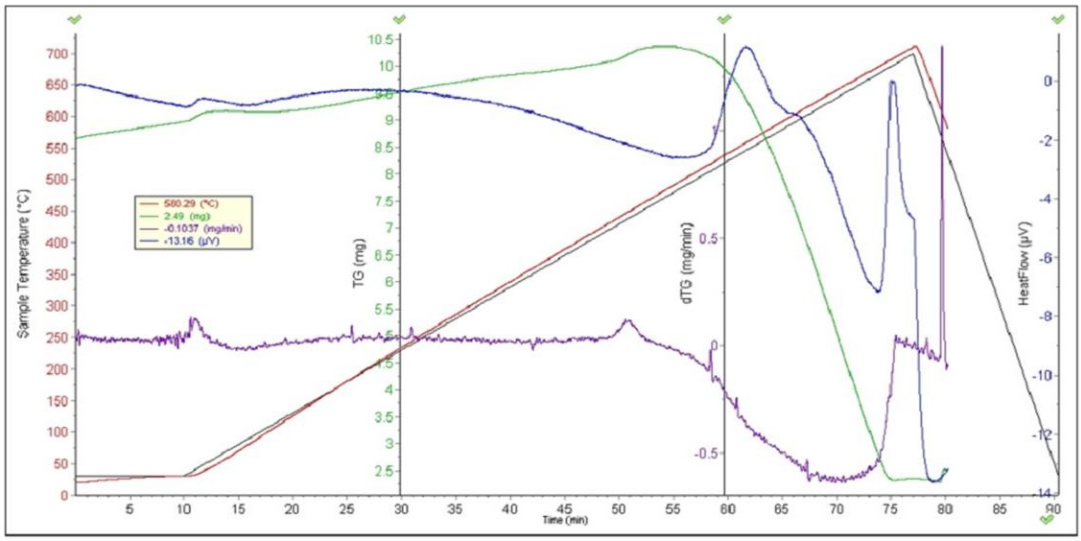

Fig. 7. TGA and DTG curves of oxygen-doped graphitic carbon nitride (O-g-C_3N_4)

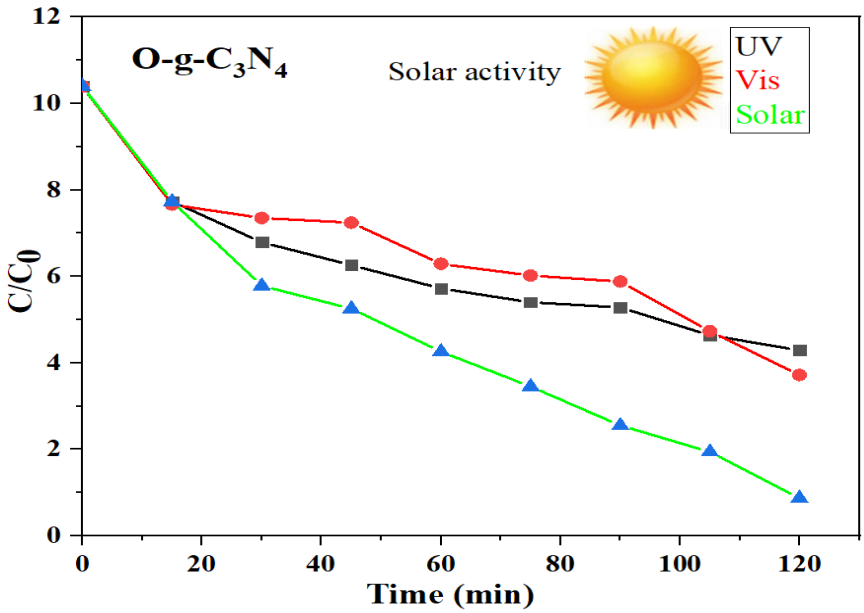

Fig. 8. Photocatalytic degradation of methylene blue over O-g-C_3N_4 under UV, visible, and solar irradiation

oxygen doping is expected to modify the electronic structure and introduce defect states, which improve charge separation and suppress recombination of photogenerated electron–hole pairs.

Upon light irradiation, electron–hole pairs are generated in the semiconductor. The photogenerated electrons react with dissolved oxygen to form superoxide radicals ($O_2^{\cdot-}$), while holes oxidize water or hydroxide ions to produce hydroxyl radicals (·OH). These reactive oxygen species play a key role in the degradation of methylene blue molecules.

Overall, the results demonstrate that O-g-C_3N_4 exhibits high photocatalytic efficiency under solar irradiation and is a promising material for the removal of organic pollutants from aqueous systems.

Kinetic analysis

The kinetics of methylene blue degradation over O-g-C_3N_4 was investigated using zero-order, first-order, and second-order kinetic models. The corresponding linear fitting plots are presented in Fig. 9a–c, and the calculated kinetic parameters are summarized in Table 2.

The zero-order kinetic model (Fig. 9a) shows a moderate linear relationship with a correlation coefficient of R^2=0.9655, indicating that the degradation process does not strictly follow zero-order kinetics.

The first-order kinetic model (Fig. 9b) exhibits the best linear fit, with a correlation coefficient of R^2=0.9892, confirming that the photocatalytic degradation of methylene blue follows a pseudo-first-order kinetic model. The corresponding apparent rate constant is k_1=0.018 min^{-1}.

In contrast, the second-order model (Fig. 9c) shows a lower correlation coefficient (R^2=0.8985), indicating a poorer agreement with the experimental data.

As shown in Table 2, the comparison of correlation coefficients clearly demonstrates that the first-order model provides the most accurate description of the degradation process. This behavior is typical for photocatalytic reactions at relatively low pollutant concentrations, where the reaction rate is primarily governed by the concentration of the organic substrate.

These results indicate that the degradation of methylene blue over O-g-C_3N_4 proceeds via surface-mediated photocatalytic reactions involving reactive oxygen species, while the concentration of active radicals remains relatively constant during the process.

Conclusions

A simple and scalable strategy for the synthesis of oxygen-doped graphitic carbon nitride (O-g-C_3N_4) was successfully demonstrated using a one-step thermal treatment in a sealed air environment, eliminating the need for inert conditions.

The obtained material combines a pseudo-layered architecture with nanoscale structural features (≈4–6 nm crystallites and ≈30 nm particle size) and oxygen-induced modification of the electronic structure. Such structural characteristics, together with a band gap of 2.64 eV, enable efficient visible-light absorption and promote improved charge carrier separation.

As a result, the photocatalyst exhibits high efficiency in methylene blue degradation, achieving nearly complete removal within 120 min under solar irradiation. The degradation process follows pseudo-first-order kinetics with a rate constant of 0.018 min^{-1}, indicating a surface-controlled photocatalytic

Table 2

Kinetic parameters of methylene blue degradation over O-g-C_3N_4 under solar irradiation

Photocatalyst	k_0	R^2 (zero-order)	k_1 (min^{-1})	R^2 (first-order)	k_2	R^2 (second-order)
O-g-C_3N_4	0.063	0.9655	0.018	0.9892	0.002	0.8985

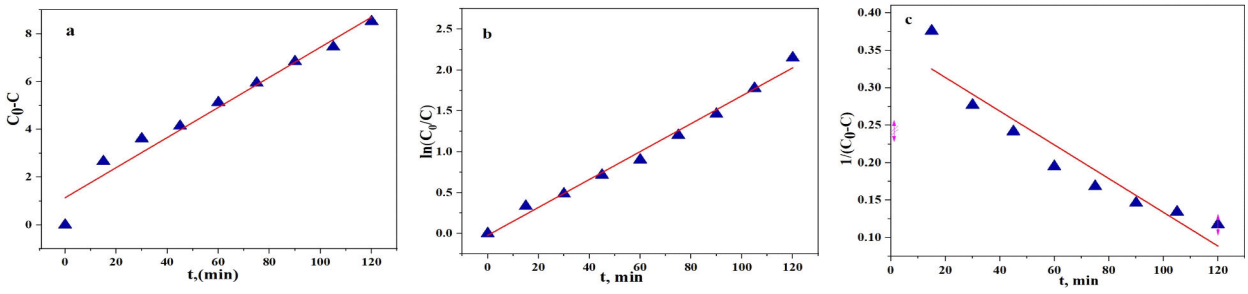

(a) (b) (c)

Fig. 9. Kinetic models for methylene blue degradation over O-g-C_3N_4: (a) zero-order; (b) pseudo-first-order; (c) second-order

mechanism.

The enhanced performance arises from the combined effect of oxygen-related defect states, which suppress recombination, and the nanoscale morphology providing accessible active sites.

Overall, the developed O-g-C_3N_4 demonstrates that combining facile synthesis with targeted electronic structure tuning is an effective strategy for designing efficient metal-free photocatalysts. The proposed approach offers strong potential for scalable applications in solar-driven water purification and environmental remediation.

REFERENCES

1. *Hignite C., Azarnoff D.L.* Drugs and drug metabolites as environmental contaminants: chlorophenoxyisobutyrate and salicylic acid in sewage water effluent // Life Sci. – 1977. – Vol.20. – P.337-341.

2. *A national* reconnaissance for pharmaceuticals and other organic wastewater contaminants in the United States – II) Untreated drinking water sources / Focazio M.J., Kolpin D.W., Barnes K.K., Furlong E.T., Meyer M.T., Zaugg S.D., et al. // Sci. Total Environ. – 2008. – Vol.402. – P.201-216.

3. *Daughton C.G., Ternes T.A.* Pharmaceuticals and personal care products in the environment: agents of subtle change? // Environ. Health Perspect. – 1999. – Vol.107. – P.907-938.

4. *Henriques J.J., Louis G.E.* A decision model for selecting sustainable drinking water supply and greywater reuse systems for developing communities with a case study in Cimahi, Indonesia // J. Environ. Manage. – 2011. – Vol.92. – P.214-222.

5. *Urban* contribution of pharmaceuticals and other organic wastewater contaminants to streams during differing flow conditions / Kolpin D.W., Skopec M., Meyer M.T., Furlong E.T., Zaugg S.D. // Sci Total Environ. – 2004. – Vol.328. – P.119-130.

6. *Heberer T.* Tracking persistent pharmaceutical residues from municipal sewage to drinking water // J. Hydrol. – 2002. – Vol.266. – P.175-189.

7. *Pharmaceuticals* and other organic waste water contaminants within a leachate plume downgradient of a municipal landfill / Barnes K.K., Christenson S.C., Kolpin D.W., Focazio M.J., Furlong E.T., Zaugg S.D., et al. // Ground Water Monit. R. – 2007. – Vol.24. – P.119-126.

8. *Halling-Sorensen B., Sengelov G., Tjornelund J.* Toxicity of tetracyclines and tetracycline degradation products to environmentally relevant bacteria, including selected tetracycline-resistant bacteria // Arch. Environ. Contam. Toxicol. – 2002. – Vol.42. – P.263-271.

9. *Hamdaoui O.* Batch study of liquid-phase adsorption of methylene blue using cedar sawdust and crushed brick // J. Hazard. Mater. – 2006. – Vol.135. – P.264-273.

10. *Futamura O., Katoh M., Takeuchi K.* Organic waste water treatment by activated sludge process using integrated type membrane separation // Desalination. – 1994. – Vol.98. – P.17-25.

11. *Bhattacharyya K.G., Sharma A.* Kinetics and thermodynamics of Methylene Blue adsorption on Neem (Azadirachta indica) leaf powder // Dyes Pigm. – 2005. – Vol.65. – P.51-59.

12. *Kinetics* and mechanism of removal of methylene blue by adsorption onto perlite / Dogan M., Alkan M., Turkyilmaz A., Ozdemir Y. // J. Hazard. Mater. – 2004. – Vol.109. – P.141-148.

13. *Heterogeneous* activation of peroxymonosulfate by supported cobalt catalysts for the degradation of 2,4-dichlorophenol in water: the effect of support, cobalt precursor, and UV radiation / Yang Q., Choi H., Chen Y., Dionysiou D.D. // Appl. Catal. B: Environ. – 2008. – Vol.77. – P.300-307.

14. *Role* of nanoparticles in photocatalysis / Beydoun D., Amal R., Low G., McEvoy S. // J. Nanopart. Res. – 1999. – Vol.1. – P.439-458.

15. *Nanosized* Co_3O_4/SiO_2 for heterogeneous oxidation of phenolic contaminants in waste water / Shukla P., Sun H., Wang S., Ang H.M., Tade M.O. // Separ. Purif. Technol. – 2011. – Vol.77. – P.230-236.

16. *Cobalt* exchanged zeolites for heterogeneous catalytic oxidation of phenol in the presence of peroxymonosulphate / Shukla P., Wang S., Singh K., Ang H.M., Tade M.O. // Appl. Catal. B: Environ. – 2010. – Vol.99. – P.163-169.

17. *Preparation* and characterization of graphitic carbon nitride through pyrolysis of melamine / Li X., Zhang J., Shen L., Ma Y., Lei W., Cui Q., et al. // Appl. Phys. A. – 2009. – Vol.94. – P.387-392.

18. *A facile* modification of g-C_3N_4 with enhanced photocatalytic activity for degradation of methylene blue / Chang F., Xie Y., Li C., Chen J., Luo J., Hu X., et al. // Appl. Surf. Sci. – 2013. – Vol.280. – P.967-974.

19. *A metal-free* and graphitic carbon nitride sonocatalyst with high sonocatalytic activity for degradation methylene blue / Song L., Zhang S., Wu X., Wei Q. // Chem. Eng. J. – 2012. – Vol.184. – P.256-260.

20. *Excellent* visible-light photocatalysis of fluorinated polymeric carbon nitride solids / Wang Y., Di Y., Antonietti M., Li H., Chen X., Wang X. // Chem. Mater. – 2010. – Vol.22. – P.5119-5121.

21. *Wang Y., Wang X., Antonietti M.* Polymeric graphitic carbon nitride as a heterogeneous organocatalyst: from photochemistry to multipurpose catalysis to sustainable chemistry // Angew. Chem. Int. Ed. – 2012. – Vol.51. – P.68-89.

22. *Laguta A., Shiknazarov A.* Colloidal stability of aqueous suspensions of bentonite clays from the krantau deposit. Analysis via dynamic light scattering // Ind. Eng. Chem. Res. – 2025. – Vol.64. – P.17658-17666.

23. *Robertson L.W., Sulkowski W., Hennig B.* Preface // Environ. Toxicol. Pharmacol. – 2008. – Vol.25. – P.127.

24. *Porta M., Zumeta E.* Implementing the Stockholm treaty on persistent organic pollutants // Occup. Environ. Med. – 2002. – Vol.59. – P.651-652.

25. *Toxic* equivalency factors (TEFs) for PCBs, PCDDs, PCDFs for humans and wildlife / Van den Berg M., Birnbaum L., Bosveld A.T., Brunstrom B., Cook P., Feeley M., et al. // Environ. Health Perspect. – 1998. – Vol.106. – P.775-792.

26. *Effects* of DEHP on endometrial receptivity and embryo implantation in pregnant mice / Li R., Yu C., Gao R., Liu X., Lu J., Zhao L., et al. // J. Hazard. Mater. – 2012. – Vol.241-242. – P.231-240.

27. *Synthesis* and thermal stability of O-g-C_3N_4/ZnO nanocomposite / Sidrasulieva G.B., Aytmuratova A.E., Kattaev N.T., Akbarov Kh.I., Tileubaev S.O., Mamatov J.Q. // Austrian J. Tech. Nat. Sci. – 2025. – No. 11-12. – P.38-43.

28. *Nanostructured* O-g-C_3N_4/ZnO composite: synthesis and morphological properties / Sidrasulieva G., Aitmuratova A., Muassarova R., Kattaev N., Akbarov Kh., Tileubaev S. // Am. J. Polym. Sci. – 2025. – Vol.14. – No. 3. – P.46-51.

29. *Oxygen* doped graphitic carbon nitride photocatalysts: physical-chemical and photocatalytic properties / Bakhromova I.A., Kattaev N.T., Akbarov Kh.I., Sidrasulieva G.B. // Eur. Chem. Bull. – 2023. – Vol.12. – No. 3. – P.1794-1804.

Received 24.03.2026
Revised 16.04.2026
Accepted 09.06.2026
Published 10.08.2026

ПРОСТИЙ СИНТЕЗ І ФІЗИКО-ХІМІЧНІ ВЛАСТИВОСТІ КИСЕНЬ-ДОПОВАНОГО ГРАФІТОПОДІБНОГО НІТРИДУ ВУГЛЕЦЮ (O-g-C_3N_4) ДЛЯ ЕФЕКТИВНОЇ ФОТОКАТАЛІТИЧНОЇ ДЕГРАДАЦІЇ МЕТИЛЕНОВОГО СИНЬОГО

Г. Сідрасулієва, Н. Каттаєв, Х. Акбаров, А. Айтмуратова, С. Уснатдінова, Дж. Маматов, С. Отажонов, Р. Муяссарова, С. Тілеубаєв

Безметалевий фотокаталізатор на основі допованого киснем графітоподібного нітриду вуглецю (O-g-C_3N_4) було синтезовано шляхом простого одностадійного термічного поліконденсування меламіну з подальшим ультразвуковим диспергуванням. Одержаний O-g-C_3N_4 характеризувався псевдошаруватою структурою та нанорозмірною морфологією. Встановлено, що ширина забороненої зони становить 2,64 еВ, що свідчить про активність у видимій області спектра. Фотокаталітичну ефективність оцінювали за ступенем деградації метиленового синього під дією сонячного випромінювання; майже повне розкладання барвника досягалося протягом 120 хв. Кінетичний аналіз показав, що процес описується моделлю псевдопершого порядку з константою швидкості 0,018 хв$^{-1}$. Підвищена фотокаталітична активність зумовлена модифікацією електронної структури, індукованою киснем, а також покращеним розділенням зарядів. Отримані результати демонструють, що O-g-C_3N_4 є ефективним безметалевим фотокаталізатором для застосування в технологіях очищення стічних вод.

Ключові слова: O-g-C_3N_4; наночастинки; морфологія; фотокаталіз; метиленовий синій; видиме світло; очищення стічних вод.

FACILE SYNTHESIS AND PHYSICOCHEMICAL PROPERTIES OF OXYGEN-DOPED GRAPHITIC CARBON NITRIDE (O-g-C_3N_4) FOR EFFICIENT PHOTOCATALYTIC DEGRADATION OF METHYLENE BLUE

*Gozzal Sidrasulieva [a], Nuritdin Kattaev [a], Khamdam Akbarov [a, *], Altinay Aytmuratova [a], Sarbinaz Usnatdinova [a], Jaykhun Mamatov [a], Sardorbek Otajonov [a], Rayhona Muyassarova [b], Sadatdin Tileubaev [c]*

[a] **Department of Chemistry, National University of Uzbekistan, Tashkent, Uzbekistan**

[b] **Department of Inorganic, Physical and Colloidal Chemistry, Tashkent Pharmaceutical Institute, Tashkent, Uzbekistan**

[c] **Department of Organic and Inorganic Chemistry, Karakalpak State University, Nukus, Uzbekistan**

[*] **e-mail: akbarov_Kh@rambler.ru**

A metal-free oxygen-doped graphitic carbon nitride (O-g-C_3N_4) photocatalyst was synthesized via a facile one-step thermal polycondensation of melamine followed by ultrasonic dispersion. The obtained O-g-C_3N_4 exhibited a pseudo-layered structure and nanoscale morphology. The optical band gap was determined to be 2.64 eV, indicating visible-light activity. The photocatalytic performance was evaluated through the degradation of methylene blue under solar irradiation, achieving nearly complete degradation within 120 min. Kinetic analysis revealed that the process follows a pseudo-first-order model with a rate constant of 0.018 min^{-1}. The enhanced photocatalytic activity is attributed to oxygen-induced modification of the electronic structure and improved charge separation. The results demonstrate that O-g-C_3N_4 is an efficient metal-free photocatalyst for wastewater treatment applications.

Keywords: O-g-C_3N_4; nanoparticles; morphology; photocatalysis; methylene blue; visible light; wastewater treatment.

REFERENCES

1. Hignite C, Azarnoff DL. Drugs and drug metabolites as environmental contaminants: chlorophenoxyisobutyrate and salicylic acid in sewage water effluent. *Life Sci.* 1977; 20: 337-341. doi: 10.1016/0024-3205(77)90329-0.

2. Focazio MJ, Kolpin DW, Barnes KK, Furlong ET, Meyer MT, Zaugg SD, et al. A national reconnaissance for pharmaceuticals and other organic wastewater contaminants in the United States — II) Untreated drinking water sources. *Sci Total Environ*. 2008; 402: 201-216. doi: 10.1016/j.scitotenv.2008.02.021.

3. Daughton CG, Ternes TA. Pharmaceuticals and personal care products in the environment: agents of subtle change? Environ Health Perspect. 1999; 107: 907-938. doi: 10.1289/ehp.99107s6907.

4. Henriques JJ, Louis GE. A decision model for selecting sustainable drinking water supply and greywater reuse systems for developing communities with a case study in Cimahi, Indonesia. *J Environ Manage.* 2011; 92: 214-222. doi: 10.1016/j.jenvman.2010.09.016.

5. Kolpin DW, Skopec M, Meyer MT, Furlong ET, Zaugg SD. Urban contribution of pharmaceuticals and other organic wastewater contaminants to streams during differing flow conditions. *Sci Total Environ*. 2004; 328: 119-130. doi: 10.1016/j.scitotenv.2004.01.015.

6. Heberer T. Tracking persistent pharmaceutical residues from municipal sewage to drinking water. *J Hydrol.* 2002; 266: 175-189. doi: 10.1016/S0022-1694(02)00165-8.

7. Barnes KK, Christenson SC, Kolpin DW, Focazio MJ, Furlong ET, Zaugg SD, et al. Pharmaceuticals and other organic waste water contaminants within a leachate plume downgradient of a municipal landfill. *Ground Water Monit R.* 2007; 24: 119-126. doi: 10.1111/j.1745-6592.2004.tb00720.x.

8. Halling-Sorensen B, Sengelov G, Tjornelund J. Toxicity of tetracyclines and tetracycline degradation products to environmentally relevant bacteria, including selected tetracycline-resistant bacteria. *Arch Environ Contam Toxicol.* 2002; 42: 263-271. doi: 10.1007/s00244-001-0017-2.

9. Hamdaoui O. Batch study of liquid-phase adsorption of methylene blue using cedar sawdust and crushed brick. *J Hazard Mater.* 2006; 135: 264-273. doi: 10.1016/j.jhazmat.2005.11.062.

10. Futamura O, Katoh M, Takeuchi K. Organic waste water treatment by activated sludge process using integrated type membrane separation. *Desalination*. 1994; 98: 17-25. doi: 10.1016/0011-9164(94)00128-6.

11. Bhattacharyya KG, Sharma A. Kinetics and thermodynamics of Methylene Blue adsorption on Neem (Azadirachta indica) leaf powder. *Dyes Pigm.* 2005; 65: 51-59. doi: 10.1016/j.dyepig.2004.06.016.

12. Dogan M, Alkan M, Turkyilmaz A, Ozdemir Y. Kinetics and mechanism of removal of methylene blue by adsorption onto perlite. *J Hazard Mater.* 2004; 109: 141-148. doi: 10.1016/j.jhazmat.2004.03.003.

13. Yang Q, Choi H, Chen Y, Dionysiou DD. Heterogeneous activation of peroxymonosulfate by supported cobalt catalysts for the degradation of 2,4-dichlorophenol in water: the effect of support, cobalt precursor, and UV radiation. *Appl Catal B Environ*. 2008; 77: 300-307. doi: 10.1016/j.apcatb.2007.07.020.

14. Beydoun D, Amal R, Low G, McEvoy S. Role of nanoparticles in photocatalysis. *J Nanopart Res.* 1999; 1: 439-458. doi: 10.1023/A:1010044830871.

15. Shukla P, Sun H, Wang S, Ang HM, Tade MO. Nanosized Co_3O_4/SiO_2 for heterogeneous oxidation of phenolic contaminants in waste water. *Separ Purif Technol.* 2011; 77: 230-236. doi.org/10.1016/j.seppur.2010.12.011.

16. Shukla P, Wang S, Singh K, Ang HM, Tade MO. Cobalt exchanged zeolites for heterogeneous catalytic oxidation of phenol in the presence of peroxymonosulphate. *Appl Catal B Environ.* 2010; 99: 163-169. doi: 10.1016/j.apcatb.2010.06.013.

17. Li X, Zhang J, Shen L, Ma Y, Lei W, Cui Q, et al. Preparation and characterization of graphitic carbon nitride through pyrolysis of melamine. *Appl Phys A.* 2009; 94: 387-392. doi: 10.1007/s00339-008-4816-4.

18. Chang F, Xie Y, Li C, Chen J, Luo J, Hu X, et al. A facile modification of g-C_3N_4 with enhanced photocatalytic activity for degradation of methylene blue. *Appl Surf Sci.* 2013; 280: 967-974. doi: 10.1016/j.apsusc.2013.05.127.

19. Song L, Zhang S, Wu X, Wei Q. A metal-free and graphitic carbon nitride sonocatalyst with high sonocatalytic activity for degradation methylene blue. *Chem Eng J*. 2012; 184: 256-260. doi: 10.1016/j.cej.2012.01.053.

20. Wang Y, Di Y, Antonietti M, Li H, Chen X, Wang X. Excellent visible-light photocatalysis of fluorinated polymeric carbon nitride solids. *Chem Mater*. 2010; 22: 5119-5121. doi: 10.1021/cm1019102.

21. Wang Y, Wang X, Antonietti M. Polymeric graphitic carbon nitride as a heterogeneous organocatalyst: from photochemistry to multipurpose catalysis to sustainable chemistry. *Angew Chem Int Ed*. 2012; 51: 68-89. doi: 10.1002/anie.201101182.

22. Laguta A, Shiknazarov A. Colloidal stability of aqueous suspensions of bentonite clays from the krantau deposit. Analysis via dynamic light scattering. *Ind Eng Chem Res*. 2025; 64: 17658-17666. doi: 10.1021/acs.iecr.5c00944.

23. Robertson LW, Sulkowski W, Hennig B. Preface. *Environ Toxicol Pharmacol*. 2008; 25: 127. doi: 10.1016/j.etap.2007.10.006.

24. Porta M, Zumeta E. Implementing the Stockholm treaty on persistent organic pollutants. *Occup Environ Med*. 2002; 59: 651-652. doi: 10.1136/oem.59.10.651.

25. Van den Berg M, Birnbaum L, Bosveld AT, Brunstrom B, Cook P, Feeley M, et al. Toxic equivalency factors (TEFs) for PCBs, PCDDs, PCDFs for humans and wildlife. *Environ Health Perspect*. 1998; 106: 775-792. doi: 10.1289/ehp.98106775.

26. Li R, Yu C, Gao R, Liu X, Lu J, Zhao L, et al. Effects of DEHP on endometrial receptivity and embryo implantation in pregnant mice. *J Hazard Mater*. 2012; 241-242: 231-240. doi: 10.1016/j.jhazmat.2012.09.038.

27. Sidrasulieva GB, Aytmuratova AE, Kattaev NT, Akbarov KhI, Tileubaev SO, Mamatov JQ. Synthesis and thermal stability of O-g-C_3N_4/ZnO nanocomposite. *Austrian J Tech Nat Sci*. 2025; (11-12): 38-43. doi: 10.29013/AJT-25-11.12-38-43.

28. Sidrasulieva G, Aitmuratova A, Muassarova R, Kattaev N, Akbarov Kh, Tileubaev S. Nanostructured O-g-C_3N_4/ZnO composite: synthesis and morphological properties. *Am J Polym Sci*. 2025; 14(3): 46-51. doi: 10.5923/j.ajps.20251403.02.

29. Bakhromova IA, Kattaev NT, Akbarov KhI, Sidrasulieva GB. Oxygen doped graphitic carbon nitride photocatalysts: physical-chemical and photocatalytic properties. *Eur Chem Bull*. 2023; 12(3): 1794-1804. doi: 10.31838/ecb/2023.12.3.130.